ORIGINAL RESEARCH

A Bayesian framework for the extraction of input function for 18F-FDG metabolism study for both healthy and infarcted rats' hearts

Rostom Mabrouk[1, 2], François Dubeau[3], Layachi Bentabet[4]

1. Centre for Addiction and Mental Health, University of Toronto, Toronto, Canada. 2. Nuclear Medicine Department, Université de Sherbrooke, Canada. 3. Mathematics Department, Université de Sherbrooke, Canada. 4. Computer Sciences Department, Bishop's University, Canada

Correspondence: Rostom Mabrouk. Address: Département médecine nucléaire et radiobiologie, Faculté de médecine et des sciences de la santé Université de Sherbrooke, Sherbrooke, Qc, J1H 5N4, CANADA. Telephone: 1-189 346-1110 ext 13152. Email: rostom.mabrouk@usherbrooke.ca.

Received: December 20, 2012 **Accepted:** March 24, 2013 **Online Published:** May 9, 2013
DOI: 10.5430/jbgc.v3n4p8 **URL:** http://dx.doi.org/10.5430/jbgc.v3n4p8

Abstract

The quantitative analysis of tracers in positron emission tomography (PET) studies requires the measurement uptake and retention of tracer in tissue over time. This analysis applied to the heart allows to diagnose its state. It could provide a means to identify areas of myocardial viability and to assess myocardial ischemia. However, the input function (IF), quite commonly used in quantitative analysis, can be corrupted by undesirable effects such as spillover. In this paper, we propose a new approach to correct the cross contamination effect on PET dynamic image sequences. It is based on the decomposition of image pixel intensity into blood and tissue components using Bayesian statistics. The method uses an a priori knowledge of the probable distribution of blood and tissue in the images. Likelihood measures are computed by a General Gaussian Distribution (GGD) model. Bayes' rule is then applied to compute weights that account for the concentrations of the radiotracer in blood and tissue and their relative contributions in each image pixel. We tested the method on a set of dynamic cardiac FDG-PET of healthy and unhealthy rats. The results show the benefit of our correction on the generation of pixel-wise images of myocardial metabolic rates for glucose (MMRG).

Key words

PET, Kinetic modeling, Input function, Bayes rule

1 Introduction

Imaging the bio-distribution and kinetics of radiopharmaceuticals with positron emission tomography (PET) is a valuable tool to assess a variety of dynamic parameters. Up to now, the invasive arterial plasma sampling procedure to obtain the IF reference remains the gold standard. This method has been intensively investigated [1-5]. Unfortunately, the plasma sampling procedure requires a number of blood samples which alter the circulation dynamics in small animals due to blood loss. The blood samples need to be measured in counters for radiotracer concentration, cross calibrated with the PET scanner, and interpolated to the image scanning times during kinetic modeling. All these operations are either invasive, cumbersome, or add uncertainties in the calculated final values. The arterial plasma can also be obtained by an automatic

blood sampling technique [6-9], which requires additional corrections. Furthermore, this method has many drawbacks such as time delay, dispersion in the tubing, contamination of the samples, and cross calibration between the sample detection setup and the PET scanner [10]. To avoid the difficulties encountered in withdrawing and measuring blood samples in each experience, population-based IFs have been introduced. In this approach, only one or a few blood samples are extracted from the subject to normalize the averaged IF [11-13]. Other authors have proposed the extraction of the IF from images [14-18]. Buvat et al. [19] have used the factor analysis of dynamic structures (FADS) method to decompose the dynamic sequences into component images. The IF is then extracted from the blood component in the images' sequence [20-22]. Independent component analysis (ICA) is another method that has been applied to extract IF from PET images [23-28]. ICA acts in similar fashion as FADS but uses a de-mixing matrix to isolate components from a mixture. In some studies [29, 30], the authors have presented a method of IF extraction from the so-called image-derived input function (IDIF). The IF can also be obtained by the simultaneous estimation method, based on a multi-exponential time-activity functions scaled to the measured activity concentration from a limited number of blood samples [31]. In some cases, cell damage in a healthy heart leads to cardiac dysfunction and hence, affects the physiologic and metabolic parameters. Consequently, the uptake and retention of the tracer will differ from the normal cells. This phenomenon is difficult to distinguish from the spillover effects due to the limitation of the scanner spatial resolution. This limitation entails two linked partial volume effect artifacts: a 'spill-out' and a 'spill-in' effect. The 'spill-out' manifests in tissue activity spreads over its surroundings, so that the measured activity is lower than the actual one. However, the 'spill-in' appears as a spills of activity from surrounding tissues into damage cell area, so that the measured activity is artificially increased. These two phenomena could be confused with the low activity produced by cell damage.

The aim of this study is to improve the approach presented [32] to correct the 18F-deoxy-fluoro-glucose (18F-FDG) PET imaging for spillover and the use of the two compartment model as presented [33] to assess the myocardial metabolism rates for glucose (MMRG). This paper considers the likelihood function as a function estimated from the spatial domain modeled by a general Gaussian distribution (GGD). Then it uses an a priori for the blood activity which is computed from a carefully withdrawn blood sample. This method was applied to healthy and unhealthy rats. The obtained results allow assessment of the extent of tissue damage due to a myocardial infarction (MI).

2 Materials and methods

2.1 PET measurements

All experiments were performed on Fischer male rats weighing 200−220g (Charles River Canada). The experiments followed a protocol approved by the Canadian Council on Animal Care and the in-house ethics committee. The experimental protocol was designed in such a way that the animals had free access to food and water throughout the studies. The study was performed on a set of normal rats and rats with MI induced by ligature of the left coronary artery. The PET scans were performed with the Sherbrooke small-animal PET scanner (LabPET4). The scanner is made of 32 avalanche photodiode detector rings and produces 63 image planes (32 direct, 31 cross) over a 3.75 cm axial field of view (FOV). The pixel size after reconstruction is 0.5mm×0.5mm×1.175 mm. The scanner has a flexible system of acquiring list-mode data that allow elaborate dynamic PET image series to be extracted as desired. Almost 60 minutes of dynamic acquisitions in list-mode were performed on the LabPET4 scanner. Radiotracer was injected via a catheter into the caudal vein. The injection of 50±5 MBq of 18F-FDG in a volume of 400 μL was done over the course of 1 minute using an automatic infusion pump in the tail vein. During the acquisition, blood was withdrawn through a femoral artery catheter at 20, 40, 50, 60, 70, 90, 120, 150, 180 sec, and at 5, 10, 15, 20, 25, 35, 52 min. The blood time-activity curves generated from sampled blood were linearly interpolated to the midpoint times of the 31 PET frames. Thirty minutes after the injection, the glucose level was obtained from the plasma analysis using a commercial reagent kit (Siemens Healthcare Diagnostic Inc., Deerfield, IL, USA) and an automated clinical chemistry analyzer (Dimension Xpand Plus, Siemens Healthcare Diagnostic Inc., IL, USA).

2.2 Methods

In order to quantify the MMRG, a mathematical framework was developed by several investigators [34, 35]. The three-compartment FDG model is used in this study for estimating the rate constants and MMRG. The model, which refers to the tissue activity measured by the scanner, is described by a set of differential equations where the solution is given by:

$$tTAC(t) = \Big(C_f(t) + C_m(t)\Big), \tag{1}$$

where

$$C_f = \left(\frac{K_1(k_4 - \alpha_1)}{\alpha_2 - \alpha_1}[(k_4 - \alpha_1)e^{-\alpha_1 t} + (\alpha_2 - k_4)e^{-\alpha_2 t}]\right) \otimes C_p,$$

and

$$C_m = \left(\frac{K_1 k_3}{\alpha_2 - \alpha_1}[e^{-\alpha_1 t} - e^{-\alpha_2 t}]\right) \otimes C_p,$$

with

$$\alpha_1, \alpha_2 = \frac{\left[k_2 + k_3 + k_4 \mp \sqrt{(k_2 + k_3 + k_4)^2 - 4k_2 k_4}\right]}{2},$$

where C_p is the IF which refers to the tracer concentration in the blood. The constant K_1 refers to the rate of delivery of the tracer to tissue in units of volume of blood per mass of tissue per minute (mL/g/min), and k_2,k_3,k_4 are the transport rate constants in units of min^{-1}. The symbol $\otimes$ in equ (1) indicates the convolution operation. The MMRG is defined by:

$$MMRG(\mu mole/100g/\text{min}) = 100\frac{gl}{LC}K, \tag{2}$$

where gl is the glycemia value in $mmol/L$, $K = \frac{K_1 k_3}{k_2 + k_3}$ the influx rate constant and LC= 1 is the lumped constant accounting for the utilization of FDG versus glucose which is the natural substrate.

Equation (1) relates to the free and the metabolic compartments of the region of interest. In practice, only the total concentration of C_f and C_m can be measured. This model was used in the case of cerebral study where the IF was extracted from the carotid region [36]. In this case, the IF extracted is free from the potential of cross contamination due to the poor surrounding tissue around the carotid. Also, the tissue activity is free of the spillover [24]. All these features made the three compartment model, as described by equ (1), a good model to assess MMRG. In the case of heart studies and especially for small animals, the spillover problem prevents the use of the model. Two different solutions can be utilized. First, the model was modified to compute the contamination of tissue by the blood activity as described in the following equation [37]:

$$tTAC(t) = \Big(C_f(t) + C_m(t)\Big) + k_5 C_p(t). \tag{3}$$

This solution is simple; however, it can lead to imprecise rate constants because the model is compromised by a high degree of parameterization, and thus leads to numerically inaccurate parameter estimates. In the case of a global MMRG estimate, the tissue activity is calculated as a mean of ROI activity over time. Averaging activity in this ROI leads to a smoothing effect. This allows minimization of the cross contamination effect and leads to the acquisition of rate values similar to those presented elsewhere in the literature. But in the case of pixel-wise imaging, the spillover and noise at the level of the voxel results in uncertainty of values. Second, IF and tissue activities are corrected for the spillover effect. For

this purpose, we introduce a new likelihood function for tissue and blood activities, and an a prior probability model for the blood activity. These probabilities are combined using a Bayesian approach [32]. Given two manually drawn ROIs as depicted in Figure 1,

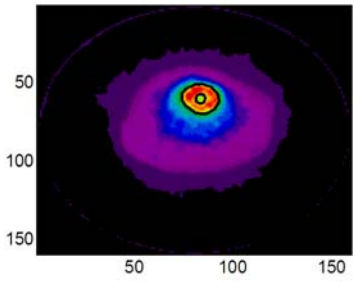

Figure 1. Image of the rat heart measured with 18F-FDG during 20min at 40min after tracer injection

We denote by S the region defined by the external contour (myocardium and left ventricle). The pixels outside this region were not considered for spillover correction. The activity within S is modeled as a random field X^t, where $t = 1, \cdots, \tau$ refers to the time index of the image frame within the sequence. The value of X^t at a point $s \in S$ is written as: x_s^t. We consider every frame measured as a mixture of two distinct components of blood and tissue activities. Consequently, X^t is modeled as a mixture of two random processes, X_B^t which models the blood component and X_T^t which models the tissue component. $S$is spatially split into two parts, S_B and S_T. Thus, we model the activity of pure blood as:

$$x_{B,s}^t = \begin{cases} \alpha_{B,s}^t x_s^t, & s \in S_B, \\ (1 - \alpha_{T,s}^t) x_s^t, & s \in S_T, \end{cases} \tag{4}$$

and we model the activity of tissue as:

$$x_{T,s}^t = \begin{cases} (1 - \alpha_{B,s}^t) x_s^t, & s \in S_B, \\ \alpha_{T,s}^t x_s^t, & s \in S_T. \end{cases} \tag{5}$$

In equ (4) and equ (5), $\alpha_{B,s}^t \in [0,1]$ and $\alpha_{T,s}^t \in [0,1]$ are the actual fractions of blood and tissue activities at each pixel $s \in S$ at time $t = 1, \cdots, \tau$. In the following, we estimate these fractions from the measured X^t using a Bayesian framework as:

$$\alpha_{B,s}^t \stackrel{\text{def}}{=} p(X_B^t | x_s^t).$$

Using the Bayes' rule one obtains

$$\alpha_{B,s}^t = \frac{p(x_s^t | X_B^t) p(X_B^t)}{\sum_{i=B,T} p(x_s^t | X_i^t) p(X_i^t)}. \tag{6}$$

Similarly, the tissue fraction is defined as:

$$\alpha_{T,s}^t \stackrel{\text{def}}{=} p(X_T^t | x_s^t),$$

then

$$\alpha_{T,s}^t = \frac{p(x_s^t | X_T^t) p(X_T^t)}{\sum_{i=B,T} p(x_s^t | X_i^t) p(X_i^t)}, \tag{7}$$

where $p(x_s^t | X_B^t)$ and $p(x_s^t | X_T^t)$ are modeled by a GGD (see Figure 2).

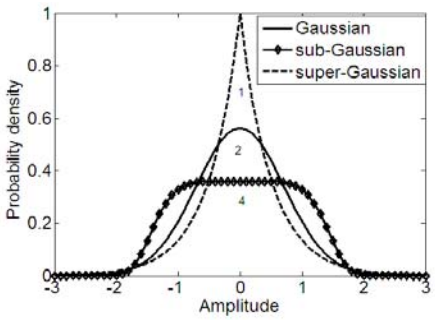

Figure 2. Generalized Gaussian distribution with fixed parameter $\mu = 0$, and $\sigma = 1$ for different values of the shape parameter.

The choice of the GGD to model the likelihood for tissue and blood activities is justified by the difference between the two structures. Blood is a fluid with homogenous cells, and tissue is formed by cells with variable responses from one another. As a result, we expect a flat p.d.f distribution for the tissue and a sharp p.d.f distribution for the blood.

The conditional p.d.f $p(x_s^t|X_i^t)$ for $i = B\ or\ T$ is given by:

$$p(x_s^t|X_i^t) = \frac{\beta_i}{2\sigma_i\Gamma\left(\frac{1}{\beta_i}\right)} e^{-\left[\frac{|x_{s,i}^t-\mu_i|}{\sigma_i}\right]^{\beta_i}} \tag{8}$$

where $x_{s,T}^t$ is a pixel belonging to the tissue ROI. The estimation of the different parameters $(\mu_i, \sigma_i, \beta_i)$ is presented in ref. 36.

The prior probability for the blood is computed from a sampled C_p curve. The curve was carefully sampled with a 5 second steps during the first 2 min of the scan. The weights over time in the Bayesian rule are calculated as follows:

$$p(X_B^t) = \begin{cases} 1 & \text{if t<2min,} \\ \frac{\mathrm{SC_p}}{\sum \mathrm{SC_p}} & \text{if t>2 min,} \end{cases} \tag{9}$$

where $\mathrm{SC_p}$ is the sampled $\mathrm{C_p}$. Figure 3 depicts the blood prior $p(X_B^t)$

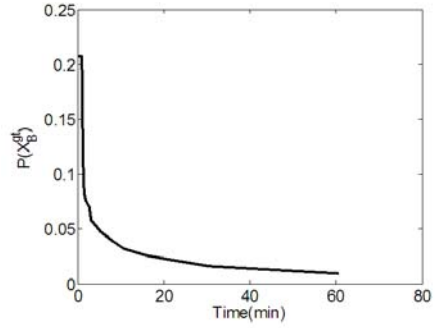

Figure 3. Prior probability of $p(X_B^t)$ after a bolus injection, the tracer diffuses into the tissue and consequently it exponentially decreases with time.

The time acquisition's frequency can also be used to calculate the prior probability. The dynamic PET data frames are acquired in time according to a predefined schedule. This schedule is represented by a time vector:

$$\Big(\underbrace{10sec, 20sec, \cdots, 120sec}_{12frames}, \underbrace{150sec, 180sec, \cdots, 300sec}_{6frames},$$

$$\underbrace{450sec, 600sec, \cdots, 1200sec}_{6frames}, \underbrace{1500sec, 1800sec}_{2frames}, \underbrace{2400sec}_{1frame}\Big)$$

The user reconstructs the images according to convenient acquisition times depending on the concentration of the tracer in the blood and the tissue. This acquisition time is very short in the beginning to localize peak tracer activity in the blood, and relatively long at the end to follow the activity in the tissue. The time vector is then sampled over two minute intervals to calculate the frames' frequency at each time step. The resulting histogram $\{h(u)\}_{u=1}^{n}$, where u is a time step index and n is the time vector size, represents the prior knowledge of the tracer's temporal behavior, $p(X_B^t)$, in the PET data. This histogram has an exponential-like shape, and hence an exponential p.d.f. can be used to fit it as:

$$p(X_B^t) = \begin{cases} \lambda e^{-\lambda t} & \text{if } t > 0, \\ 0 & \text{if } t < 0, \end{cases} \tag{10}$$

where λ is a positive parameter that is estimated with maximum likelihood estimator as follows:

$$\lambda = \frac{n}{\sum_{u=1}^{n} h(u)}$$

The tissue prior $p(X_T^t)$, depicted in Figure 4, is computed from the FDG model as the response of tissue after a bolus injection. It follows from equ (1):

$$p(X_T^t) = \frac{K_1}{\alpha_1 + \alpha_2}\left[(k_3 + k_4 - \alpha_1)e^{(-\alpha_1 t)}(\alpha_2 - k_3 - k_4)e^{(-\alpha_2 t)}\right] \otimes p(X_B^t)\,, \tag{11}$$

where K_1=0.102 ml/min/g , k_2= 0.13 min^{-1}, k_3 = 0.062 min^{-1}, and k_4= 0.0068 min^{-1}. These parameter values are representative of those usually obtained from studies in normal subjects.

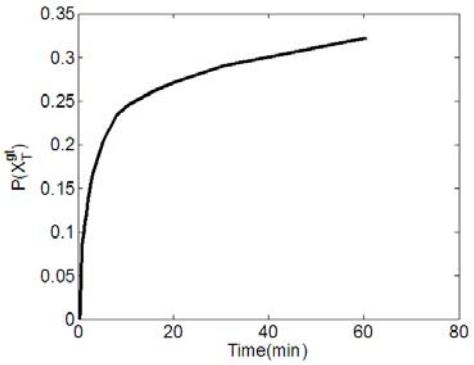

Figure 4. Prior probability of $p(X_T^t)$. The PET measurement in a tissue is viewed as the cumulative uptake response of the radiotracer diffused by blood

Our approach is summarized in Figure 5, which depicts how the initial PET image is processed to find the blood fraction and the tissue fraction images.

Once the component images are calculated, the time activity curve of each component is easily obtained as the average intensity. For the blood component, the time activity curve corresponds to the whole blood and it is calculated as follows:

$$C_w(t) = \frac{1}{N}\sum_{s \in S} x_{B,s}^t. \tag{12}$$

The plasma activity curve, $C_p(t)$, is then obtained from the whole blood activity, $C_w(t)$, using a correction factor $R_{BP}(t)$ as follows:

$$C_p(t) = R_{BP}(t)C_w(t), \tag{13}$$

where R_{BP} is calculated by taking a series of whole-blood samples throughout the course of several studies, centrifuging each sample into plasma and cellular components, and measuring the FDG concentration in each fraction. The resulting R_{BP} is time dependent [37, 38]:

$$R_{BP}(t) = 0.386e^{(-0.191\,t)} + 1.165. \tag{14}$$

For the tissue component, the time activity curve is calculated as follows:

$$tTAC(t) = \frac{1}{N}\sum_{s\in S} x_{T,s}^t \ . \tag{15}$$

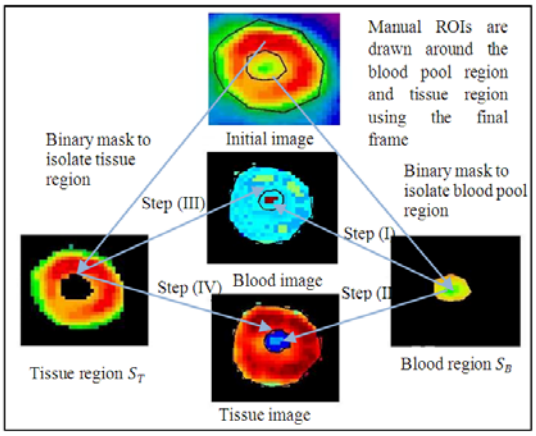

Figure 5. Procedure for calculating the blood images and tissue images. Step (I) is the calculation of the blood fraction from the intensity of a pixel belonging to the blood pool region as $x_{B,s}^t = \alpha_{B,s}^t \cdot x_s^t$. The remaining intensity will be allocated to the same location for the tissue image in step (II) as $x_{T,s}^t = (1 - \alpha_{T,s}^t) \cdot x_s^t$. Similarly, for a pixel belonging to the tissue region, we calculate in step (III) the fraction of blood as $x_{B,s}^t = (1 - \alpha_{B,s}^t) \cdot x_s^t$ and the fraction of tissue for the same pixel as $x_{T,s}^t = \alpha_{T,s}^t x_s^t$ in step (IV).

3 Results

Our approach allowed us to isolate the fractions of blood and tissue in each pixel of the PET image. The extracted blood sequences were then used to compute $C_p(t)$ by applying a Bayesian correction on the manually segmented ROIs. The calculated IF is compared in Figure 6 with the curves obtained from the original image (ROI-IF) and the sampled curve (Sampled IF). Figure 6 shows the separation of the blood and the tissue signals. The differences between these IFs illustrate the effect of spillover in the ROI-IF, which appears during the last thirty-five minutes of the scan. The peak's location is nearly the same for all the curves. In addition, in comparison with the ROI-IF curve, the peak obtained using our approach is much higher due to the difference between whole-blood and plasma radioactivities which is corrected using equ (13).

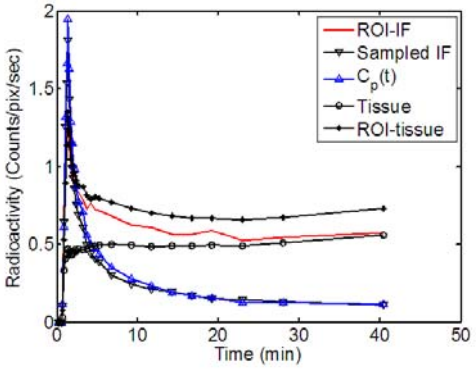

Figure 6. Time activity curves from the same rat. Comparison illustrated clearly shows the close shape of the computed $C_p(t)$ to the sampling IF. In contrast spillover appears in the ROI-IF curve especially at the end of the measure, while the tissue activity calculated from uncorrected images shows a peak at the early time of acquisition which is due to the cross contamination.

One common method to assess a global MMRG value uses just one $tTAC$ calculated as a mean for the whole myocardium. Figure 7 illustrates kinetic modeling using equ (1) for $tTAC$ obtained from original image as the average of the tissue ROI activities and equ (3) for $tTAC$ obtained from the corrected image .

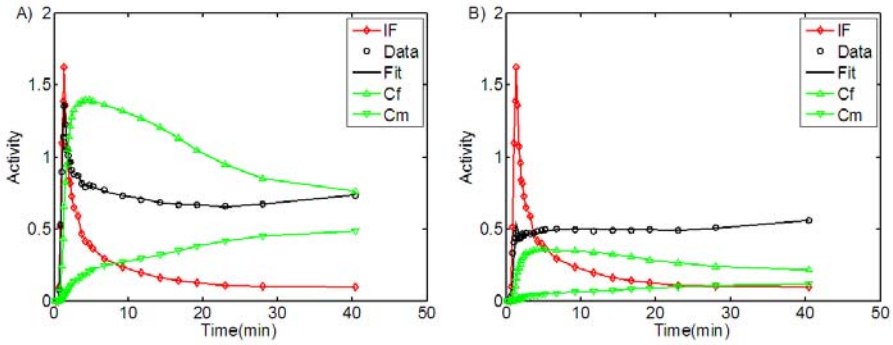

Figure 7. A nonlinear least squares fitting of $tTAC$ by the three compartment model. (A) $tTAC$ is computed from original image as mean of tissue ROI activities. (B) $tTAC$ is computed from corrected image as a mean of tissue ROI activities.

Figure 7(A) clearly shows an early peak in the tissue. The data fit gives an inaccurate shape for both free and metabolized tracers. In contrast, in Figure 7(B) the second term in equ (3), which refers to the fractional contribution of blood in tissues, is omitted. This simplification is due to the correction made in the tissue activity over the time.

In order to study the robustness of the method with respect to the ROI, two processes have been applied and tested. In the first one,100 random contours were generated from a manually traced contour around the blood pool within an area of 2 mm containing the manually drawn contour. The experiment showed a minimal change in MMRG value (standard deviation =1,15 μmole/100g/min). The second test consisted of two experts drawing eighteen healthy subjects ROIs, (the principal author and a nuclear medicine physician). The result showed that the variation of the area under curve (AUC) is minimal as illustrated in Table 1 below.

Table 1. Relative error between AUC computed by user 1 and AUC computed by user 2 calculated as $\left|\frac{AUC1-AUC2}{AUC1}\right| \times 100$. The coefficient of correlation between the AUCs values is 99.6% which proves a high reproducibility of ROI choice.

Rat index	1	2	3	4	5	6	7	8	9
Error of AUC(%)	3.0	2.8	3.5	7.6	0.4	1.5	3.2	3.1	1.8
Rat index	10	11	12	13	14	15	16	17	18
Error of AUC(%)	3.6	2.3	0.4	0.2	0.3	3.8	1.3	2.7	1.0

The MMRG values for the healthy rats are computed separately using $C_p(t)$, the sampled IF and the ROI-IF. The results are reported as box plots in Figure 8.

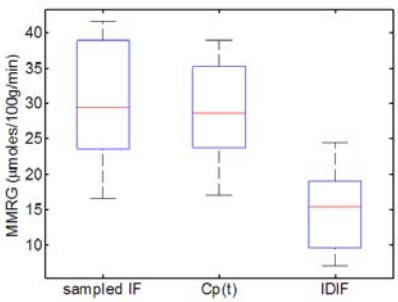

Figure 8. Comparison of FDG MMRG values obtained with the sampled IF, the ROI-IF (IDIF) and the computed $C_p(t)$ for the healthy rats. The t-test between MMRG of the sampled IF and $C_p(t)$ shows no significant difference (p<5%). The t-test between the sampled IF and the IDIF shows a significant difference (p> 5%).

The *t*-test between MMRG calculated with sampled IF and $C_p(t)$shows no significant difference (p<0.05). On the other hand, the *t*-test between MMRG calculated with the sampled IF and calculated with the ROI-IF shows a significant difference (p> 0.05). We can interpret quantitatively the difference existing in the MMRG values by computing relative errors between calculated MMRG. Indeed, the value calculated by our method differs by 3.5% from the gold standard; whereas, the value calculated with IDIF differs by 64%.

The global MMRG assessment is not, however, a reliable method to study the viability of different areas of the heart. The method is used as an indicator of the global function of the organ. In contrast, the production of MMRG value at each voxel allows a good prediction of the viability of the tissue. Figure 9 depicts parametric images calculated with and without correction of tissue activity. Figure 9(B) illustrates the importance of correction for tissue activity. Indeed, the parametric image has a good contrast and the estimated MMRG values appear as expected for a healthy heart. In Figure 9(A) the unit of glucose metabolism is poorly visualized due to the effect of the cross contamination in the original image.

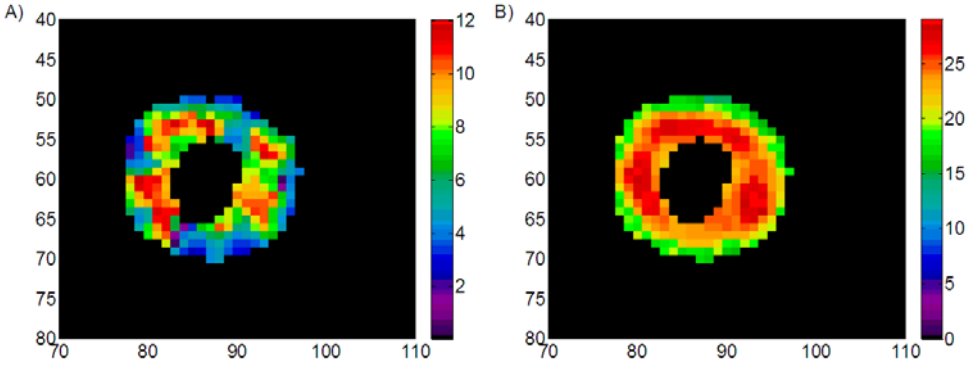

Figure 9. Parametric MMRG image. Images are resized directly in units of glucose metabolism (micromole/100g/min). (A) Parametric MMRG image computed with original images. (B) Parametric MMRG image computed with corrected images.

In the case of MI induced by ligature of the left coronary artery, which delivers glucose to the myocardium, we expect to obtain a lower unit of MMRG on the parametric image. Figure 10 illustrates glucose uptake pixel-by-pixel calculated on corrected and uncorrected tissue activity. Figure 10(A) illustrates the effect of cross contamination on the calculated MMRG value. The contrast is lower than the one in the image calculated with corrected $tTAC$. Figure 10(B) clearly depicts the extent of damaged tissue.

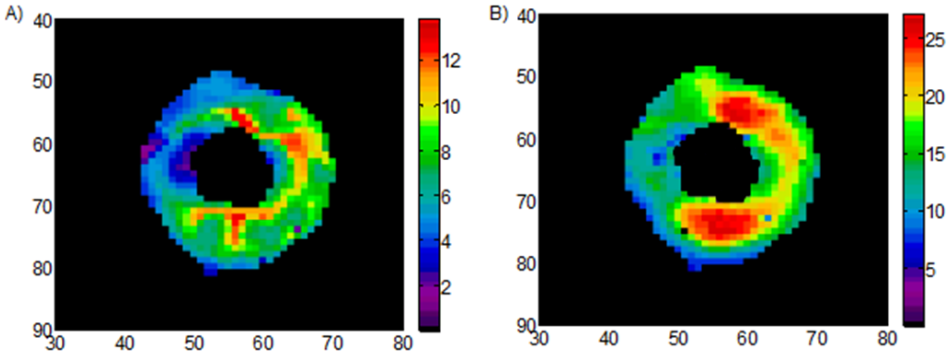

Figure 10. Parametric MMRG image for infarcted heart. (A) Parametric MMRG image computed with corrected images (B) Parametric MMRG image computed with uncorrected images.

 ISSN 1925-4008 E-ISSN 1925-4016

4 Discussion

The ability to accurately define IF is crucial for PET imaging research. In this regard, compartment modeling has long been the best way to analyze PET images. However, the blood-sampling procedure is still the reference in research. In small animals, this method has been a major barrier because of its invasive nature, the small size of blood vessels, and the animals' limited blood volume. Alternative solutions to obtain $C_p(t)$ from images include the IDIFs, the FADS and ICA. Among these methods some do not require any blood sampling and others need just one sample to calibrate the IF. ICA was mostly used in human brain PET imaging and cardiac PET imaging. Nevertheless, ICA has some pitfalls. First, the ambiguity of the sign. Hence, this method could not assure the sign of each independent source. The reason is that, both sources and mixing matrix being unknown, any scalar multiplier in one of the sources could always be cancelled by dividing the corresponding column coefficient of mixing matrix by the same scalar. The application of this method on PET images to extract blood and tissue sources could yield sometimes to a projection of component in the negative space, which requires a multiplication by (-1) as in the EPICA algorithm [24]. Second, the order of the identified independent components cannot be determined by the algorithm itself, requiring the intervention of an expert observer. Furthermore, as mentioned by Naganawa [22], the signal of the estimated IF sometimes contains negative values in a portion of the curve, which requires more complex corrections or the use of alternative methods.

The FADS algorithm is another method, which has been widely used to extract time activity curves from PET and SPECT images. However, it also suffers from data negativity problems, and statistical tools such as oblique analysis have to be used to project negative data into positive space. In contrast, IDIFs offer a very simple way to define $C_p(t)$ and tissue uptake. The disadvantage of this method is that the spillover effects make the IDIF a highly biased estimate as shown in Figure 6. All these methods require the use of a recovery coefficient to compensate for the lack of resolution of the PET scanner versus the size of the vascular structure chosen for the input function substitute. The probabilistic approach described in this paper offers a practical and robust method to correct the cross contamination by estimating the fractions of free blood and free tissue activities from the initial PET image data sequence. The results reported in Figure 6 show that the computed $C_p(t)$ is a valid and reliable estimate of the IF, and thus it can be used to accurately derive K_1, $k_2 - k_4$ and MMRG values. It does not rely on recovery coefficients. To illustrate how our method could be useful in the context of a medical diagnosis, we built parametric images for healthy and unhealthy rats which describe the MMRG value for each tissue pixel. The results are given in Figure 9 and Figure 10. MMRG parametric images reflect the rate of glucose metabolism directly, rather than the radiotracer's concentration. The MMRG parametric image in Figure 9(A) is computed using the sampled IF and x_s^t at each pixel$s \in S_T$. This image corresponds to the MMRG before the correction for spillovers. The MMRG parametric image in Figure 9(B) is computed using the sampled IF and $x_{s,T}^t$ at each pixel$s \in S_T$. This image corresponds to the MMRG after the correction for cross contamination. In the case where no correction is applied to the image sequence, the estimated MMRG is very low as indicated in Figure 9(A). This is due to inadequate estimates of constants K_1, $k_2 - k_5$ from initial PET data shown in Figure 1. By reducing the cross contamination using our approach, we obtain MMRG values suitable for medical diagnosis as shown in Figure 10(B).

The probabilistic approach described in this paper is easy to implement as standalone software or integrated into an existing one. In this work, we used the ventricular cavity activity as an IF; but, the algorithm could be used as well for the femoral and carotid arteries.

5 Conclusion

We showed that the probabilistic estimations of the blood and the tissue activities have an important benefit in the production of parametric images. Moreover, the MMRG parametric image has the advantage of simplifying the numerical evaluation of myocardial metabolism, and the compression of several image frames of dynamic PET studies.

Acknowledgment

The authors wish to thank Jean François Boudoin (Eng) from the Nuclear Medicine and Radiobiology Department at Université de Sherbrooke (Québec, Canada) for providing the data used in the experiments and Kelly Aminian from PET Centre, Centre for addiction and Mental Health, University of Toronto for her rich discussion and help.

References

[1] Greuter HN, Boellaard R, Van Lingen A, Franssen EJF, Pharm D, Lammertsma A.A. Measurement of 18F-FDG Concentrations in Blood Samples: Comparison of Direct Calibration and Standard Solution Methods. J Nucl Med Technol. 2003; 31: 206–209. PMid:14657286

[2] Abraham A, Nichol GK, Williams A, Guo A, Dekemp RA, Garrard L, Davies RA, Duchesne L, Haddad H, Chow B, Dasilva J, Beands RS. FDG PET Imaging of Myocardial Viability in an Experienced Center with Access to FDG and Integration with Clinical Management Teams: The Ottawa-FIVE Substudy of the PARR 2 Trial. J Nucl Med. 2010; 51: 567–574. PMid:20237039 http://dx.doi.org/10.2967/jnumed.109.065938

[3] Bedford RF, Wollman H. Complications of percutaneous radial-artery cannulation: an objective prospective study in man. Anesthesiology. 1973; 38: 28–36. PMID:4698143. http://dx.doi.org/10.1097/00000542-197303000-00006

[4] Jons PH, Ernst M, Hankerson J, Hardy K, and Zametkin AJ. Follow-up of radial arterial catheterization for positron emission tomography studies. Hum Brain Mapp. 1997; 5: 19–23. PMID:10096416. http://dx.doi.org/10.1002/(SICI)1097-0193(1997)5:2<119::AID-HBM5>3.0.CO;2-6

[5] Bentourkia M, Bol A, Ivanoiu A, Michel C, Coppens A, Sibomana M, Cosnard G, De Volder AG. A standardized blood sampling scheme in quantitative FDG-PET studies. IEEE Trans Med Imag. 1999; 18: 379–84. PMid:10416799 http://dx.doi.org/10.1109/42.774165.

[6] Erikson L, Kanno I. Blood sampling devices and measurements. Med Prog Tech. 1991; 17: 249–57. PMID:1839858.

[7] Munk OL, Bass L. A method to estimate dispersion in sampling catheters and to calculate dispersion-free blood time-activity curves.Med Phys. 2008; 35: 3471–3481. PMid:18777907 http://dx.doi.org/10.1118/1.2948391

[8] Senda M, Nishizawa S, Yonekura Y, Mukai T, Saji H, Konishi J, Torizuka K. Measurement of arterial time-activity curve by monitoring continuously drawn arterial blood with an external detector: errors and corrections. Ann Nucl Med. 1988; 2: 7–12. PMid:3275106 http://dx.doi.org/10.1007/BF03164580

[9] Boellaard R, Lingen A, Balen SC, Hoving BG, Lammertsma AA. Characteristics of a new fully programmable blood sampling device for monitoring blood radioactivity during PET. Eur J Nucl Med. 2001; 28: 81–89. PMid:11202456 http://dx.doi.org/10.1007/s002590000405

[10] Convert L, Brassard GM, Cadorette J, Archambault M, Bentourkia M, Lecomte R. A new tool for molecular imaging: the microvolumetric {beta} blood counter. J Nucl Med. 2007; 48: 1197–2006. PMid:17574990 http://dx.doi.org/10.2967/jnumed.107.042606.

[11] Dhawan V, Jarden JO, Strother S, Rottenberg DA. Effect of blood curve smearing on the accuracy of parameter estimates obtained for 82Rb/PET studies of blood-brain barrier permeability. Phys Med Biol. 2008; 33: 61–74. http://dx.doi.org/10.1088/0031-9155/33/1/006.

[12] Takikawa S, Dhawan V, Spetsieris P, Robeson W, Chaly T, Dahl R, Margouleff D, Eidelberg D. Noninvasive quantitative fluorodeoxyglucose PET studies with an estimated input function derived from a population-based arterial blood curve. Radiology. 1993; 188: 131–136. PMid:8511286.

[13] Eberl S, Anayat AR, Fulton RR, Hooper PK, Fulham MJ. Evaluation of two population-based input functions for quantitative neurological FDG PET studies. Eur J Nucl Med. 1997; 24: 299–304. PMID:9143468.

[14] Wakita K, Imahori Y, Ido T, Fujii R, Horii H, Shimizu M, Nakajima S, Mineura K, NakamuraT, Kanatsuna T. Simplification for measuring input function of FDG PET: investigation of 1-point blood sampling method. J Nucl Med. 2000; 41: 1484–1490. PMID:10994726.

[15] Gambhir S, Schwaiger M, Huang SC, Krivokapich J, Schelbert H, Nienaber C, Phelps ME. Simple noninvasive quantification method for measuring myocardial glucose utilization in humans employing positron emission tomography and fluorine-18 deoxyglucose. J Nucl Med. 1989; 30: 359–366. PMID:2786939.

[16] Iida H, Rhodes G, Silva R, Araujo L, Bloomfield P, Lammertsma AA, Jones T. Use of the left ventricular time-activity curve as a noninvasive input function in dynamic oxygen-15-water positron emission tomography. J Nucl Med. 1992; 33: 1669–1677. PMID:1517842.

[17] Ferl GZ, Zhang X, Wu HM, Huang SC. Estimation of the 18F-FDG input function in mice by use of dynamic small-animal PET minimal blood sample data. J Nucl Med. 2001; 42: 1622–1629. PMID:18006615.

[18] Kim J, Herrero P, Sharp T, Laforest R, Rowland DJ, Tai YC, Lewis JS, Welch MJ. Minimally invasive method of determining blood input function from PET images in Rodents. J Nucl Med. 2006; 47: 330–336. PMID:16455640.

[19] Buvat I, Benali H, Rouin F, Bazin JP, Di-Paola R. Target apex-seeking in factor analysis of medical image Sequences. Phys Med Biol. 1993; 38: 123–138. http://dx.doi.org/10.1088/0031-9155/38/1/009.

[20] Wu HM, Huang SC, Allada V, Wolfenden PJ, Schelbert HR, Phelps ME, Hoh CK. Derivation of input function from FDG-PET studies in small hearts J Nucl Med. 1996; 37(10): 1717-1722. PMID:8862318.

[21] Sitek EV, Bella D, Gullberg GT. Factor analysis with a priori knowledge - application in dynamic cardiac SPECT. Phys Med Biol. 2000; 45: 2619–2638. PMID:11008961. http://dx.doi.org/10.1088/0031-9155/45/9/314

[22] Hsiao-Ming W, Hoh KC, Choi RY, Schelbert HR, Randall RA, Phelps ME, Huang SC. Factor Analysis for Extraction of Blood Time-Activity Curves in Dynamic FDG-PET Studies. J Nucl Med. 1995; 36: 1714–1722. PMID:7658236.

[23] Naganawa M, Matani A, Kimura Y. Extraction of vessel-related information from PET images without continuous blood sampling using modified independent component analysis. Proceeding of the 23rd Annual International Conference of the IEEE Engineering in Medicine and biology Society, Istanbul. 2001; 3: 2744 –2747.

[24] Naganawa M, Kimmura Y, Oda K, Ishiwata K, Matani A. Extraction of a plasma time-activity curve from brain PET images based on independent component analysis. IEEE Trans Biomed Eng. 2005; 52: 201–210. PMID:15709657. http://dx.doi.org/10.1109/TBME.2004.840193

[25] Naganawa M, Kimmura Y, Ischii K, Oda K, Ishiwata K. Temporal and special blood information estimation using Bayesian ICA in dynamic cerebral positron emission tomography. IEEE Digital Sign Processing. 2007; 17: 973–993. http://dx.doi.org/10.1016/j.dsp.2007.03.002.

[26] Naganawa M, Tsukada H, Ohba H, Ishiwata K, Seki C, Shidahara M, Kimura Y. Omission of serial arterial blood sampling for quantitative analysis of monkey PET data using independent component analysis-based method. IEEE Nucl Sci Symp Conference Record, 2007

[27] Su KH, Lee JS, Li JH, Yang YW, Liu RS, Chen JC. Partial volume correction of the microPET blood input function using ensemble learning independent component analysis. Phys Med Biol. 2009; 54: 1823–1846. PMID:19258684. http://dx.doi.org/10.1088/0031-9155/54/6/026

[28] Mendez MM, Juslin A, Nesterov VS, Kalliokoski K, Knuuti J, Ruotsalaine U. ICA Based Automatic Segmentation of Dynamic H215O Cardiac PET Images. IEEE Trans on Inform tech in Biomed. 2010; 14: 795–802. http://dx.doi.org/10.1109/TITB.2007.910744.

[29] Van der Weerdt AP, Klein LJ, Boellaard R, Visser CA, Visser FC, Lammertsma AA. Image-derived input functions for determination of MRGlu in cardiac 18F-FDG PET scans. J Nucl Med. 2001; 42: 1622–1629. PMID:11696630.

[30] Fang Y, Muzic R. Spillover and partial-volume correction for image-derived input functions for small-animal 18F-FDG PET Studies. J Nucl Med. 2008; 49: 606–614. PMID:18344438. http://dx.doi.org/10.2967/jnumed.107.047613

[31] Wong KP, Feng D, Meikle SR, Fulham MJ. Simultaneous estimation of physiological parameters and the input function in vivo PET data. IEEE Trans Inform on Tech in Biomed. 2001; 5: 67–76. http://dx.doi.org/10.1109/4233.908397.

[32] Mabrouk R. Dubeau F, Bentourkia M, Bentabet L. Extraction of time activity curves from gated FDG-PET images for small animals' heartstudies. Comput Med Imaging Graph. 2012; 36: 484–491. PMID:22658459. http://dx.doi.org/10.1016/j.compmedimag.2012.05.002

[33] Phelps ME, Huang SC, Hoffman EJ, Selin C, Sokoloff L, Kuhl DE. Tomographic measurement of local cerebral glucose metabolic rate in humans with (F-18)2-fluoro-2-deoxy-d-glucose: validation of method. Annals of neurology. 1979; 6: 371–88. PMID:117743. http://dx.doi.org/10.1002/ana.410060502

[34] Patlak CS and Blasberg RG. Graphical evaluation of blood-to-brain transfer constants from multiple-time uptake data. Generalizations. J Cereb Blood Flow Metab. 1985; 5: 584–590. PMID:4055928. http://dx.doi.org/10.1038/jcbfm.1985.87

[35] Dennis V, Visser EP, Geus-Oei LF, Oyen Wim J.G. Methodological considerations in quantification of oncological FDG PET studies. Eur J Nucl Med Mol Imaging. 2010; 37: 1408–1425. http://dx.doi.org/10.1007/s00259-009-1306-7

[36] Chen K, Chen X, Renaut R, Alexander GE, Bandy D, Guo H, Reiman EM. Characterization of the image-derived carotid artery input function using independent component analysis for the quantitation of [18F] fluorodeoxyglucose positron emission tomography images. Phys Med Biol. 2007; 52: 7055–7071. PMID:18029993. http://dx.doi.org/10.1088/0031-9155/52/23/019

[37] Arjhoul L, Bentourkia M. Assessment of glucose metabolism from the projections using the wavelet technique in small animal pet imaging. CMIG. 2007; 31: 157–165. PMID:17276657.

[38] Mabrouk R, Dubeau F, Bentabet L. Dynamic Cardiac PET Imaging: Extraction of Time-Activity Curves using ICA and a Generalized Gaussian Distribution Model. Trans Biomed Eng. 2013; 60: 63–71. PMID:23060316. http://dx.doi.org/10.1109/TBME.2012.2221463

[39] Raymond F, Muzic J, Cornelius S. COMKAT: Compartment Model Kinetic Analysis Tool. J Nucl. Med. 2001; 42: 636–45. PMID:11337554.

[40] Wu HM, Guodong S, Lee C, Prins M, Ladno W, Lin H, Yu A, Phelps ME, Huang SC. Mouse plasma and whole blood difference in 2-[18F]fluoro-2-deoxy-D-glucose (18F-FDG) concentration: implication for quantitative mouse 18F-FDG PET studies. J Nucl Med. 2007; 48: 837–845. http://dx.doi.org/10.2967/jnumed.107.041061.